The Impacts of Wildfires on Ozone Production and Boundary Layer Dynamics in California's Central Valley

Keming Pan[1] and Ian C. Faloona[1]

[1]University of California, Davis

November 21, 2022

Abstract

We investigate the role of wildfire smoke on ozone photochemical production ($P(O_3)$) and atmospheric boundary layer (ABL) dynamics in California's Central Valley during June-September, 2016-2020. Wildfire events are identified by the Hazard Mapping System (HMS) and Hybrid Single Particle Lagrangian Integrated Trajectory Model (HYSPLIT). Air quality and meteorological data are acquired from 10 monitoring sites operated by the California Air Resources Board (CARB) across the Central Valley. During wildfire influenced periods, maximum daily 8h averaged (MDA8) O_3 was enhanced by about 5 ppb (~10%) across the entire valley after the temperature correction. The photochemical ozone production rate calculated from a modified Leighton relationship was also found to be higher by 35% on average compared to non-fire periods despite the average diminution of by ~7% due to the shading effect of the wildfire plumes. Furthermore, the in-situ ozone production rates are found to be elevated due to an increase of both peroxyl radicals (~24%) and NO (~11%). Surface heat flux measurements from two AmeriFlux sites in the Northern San Joaquin Valley show midday surface buoyancy fluxes decrease by 30% on average when influenced by wildfire smoke. Further, ABL height measured from a radio acoustic sounding system (RASS) located in Visalia in the Southern San Joaquin Valley were found to decrease 80 m and virtual potential temperatures in ABL are higher on average by ~1.5 K when wildfire smoke is present. The increased temperature is likely the result of shortwave-radiation absorption by the additional aerosols in the wildfire smoke.

The Impacts of Wildfires on Ozone Production and Boundary Layer Dynamics in California's Central Valley

Keming Pan and Ian C. Faloona

Department of Land, Air, & Water Resources and the Air Quality Research Center, University of California, Davis

Key Points:

- 5 years observation of summer time wildfire events indicate that ozone level enhanced in California's Central Valley by about 5 ppb.

- Ozone production rates are estimated to be 35% higher during wildfire periods due to the increased organic peroxyl radicals and NO.

- Daytime surface buoyancy flux decreased by 30% and ABL heights were reduced up to 80m on average due to the shading effect of wildfire smoke.

Abstract. We investigate the role of wildfire smoke on ozone photochemical production ($P(O_3)$) and atmospheric boundary layer (ABL) dynamics in California's Central Valley during June-September, 2016-2020. Wildfire events are identified by the Hazard Mapping System (HMS) and Hybrid Single Particle Lagrangian Integrated Trajectory Model (HYSPLIT). Air quality and meteorological data are acquired from 10 monitoring sites operated by the California Air Resources Board (CARB) across the Central Valley. During wildfire influenced periods, maximum daily 8h averaged (MDA8) O_3 was enhanced by about 5 ppb (~10%) across the entire valley after the temperature correction. The photochemical ozone production rate calculated from a modified Leighton relationship was also found to be higher by 35% on average compared to non-fire periods despite the average diminution of $j(NO_2)$ by ~7% due to the shading effect of

25   the wildfire plumes. Furthermore, the in-situ ozone production rates are found to be elevated due

26   to an increase of both peroxyl radicals (~24%) and NO (~11%). Surface heat flux measurements

27   from two AmeriFlux sites in the Northern San Joaquin Valley show midday surface buoyancy

28   fluxes decrease by 30% on average when influenced by wildfire smoke. Further, ABL height

29   measured from a radio acoustic sounding system (RASS) located in Visalia in the Southern San

30   Joaquin Valley were found to decrease 80 m and virtual potential temperatures in ABL are

31   higher on average by ~1.5 K when wildfire smoke is present. The increased temperature is likely

32   the result of shortwave-radiation absorption by the additional aerosols in the wildfire smoke.

33

35

36   **Plain Language Summary**

37   Ozone is a gas composed of three atoms of oxygen and is known to harm human health
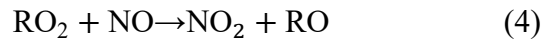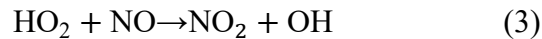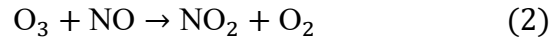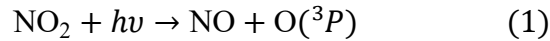
38   and ecosystem if it is present in high concentration at ground level. Most ground level

39   ozone is produced by chemical reactions between nitrogen oxides and volatile organic

40   compounds in the presence of sunlight. Ozone pollution is still a problem in California's

41   Central valley region during the summer season and wildfires tend to occur at the same

42   time. When the wildfire smokes are transported to urban regions, they can influence ozone

43   production processes by providing additional volatile organic compounds and nitrogen

44   oxides thus complicating our understanding of pollution induced ozone. In our study, we

45   use satellite-based product and a dynamic model product to identify wildfire events.

46   According to the measurements of pollutants, we find that the concentration of particulate

47   matter, carbon monoxide, ozone and nitrogen oxides exhibit prominent enhancements, and

48   the ozone production rate is found to increase by 35% during wildfire influenced periods.

49   Wildfire smoke also blocks the sunlight that heats the earth's surface and thereby

50   suppresses the buoyant forcing of the convectively mixing air, by roughly 30% leading to

51   mixed layers that were about 12% more shallow compared to non-fire days.

52

1. Introduction

54   Ozone (O_3) pollution possesses a threat to public health and the environment. It could damage

55   the tissues of respiratory tracts, causing a variety of symptoms, such as chest pain, coughing,

56   throat irritation and worsening emphysema, asthma, leading to increased medical care (Rombout

57   et al., 1986). Apart from that, ozone also causes substantial damage to crops, forest, and native

58   plants (Ainsworth, 2017). Tropospheric ozone is produced from the chemical reaction of

59   nitrogen oxides ($NO_x=NO+NO_2$) and volatile organic compounds (VOCs) in the presence of

60   sunlight, Figure 1 shows the schematic representation of the photochemical formation of ozone

61   in the presence of NO_x and VOCs (Amann, 2018). Equation (1)-(5) are the major reactions in

62   this process.

$$NO_2 + h\upsilon \rightarrow NO + O(^3P) \qquad (1)$$

$$O_3 + NO \rightarrow NO_2 + O_2 \qquad (2)$$

$$HO_2 + NO \rightarrow NO_2 + OH \qquad (3)$$

$$RO_2 + NO \rightarrow NO_2 + RO \qquad (4)$$

$$O_2 + O(^3P) + M \rightarrow O_3 + M \qquad (5)$$
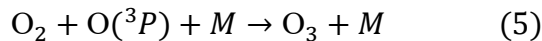
63   Wildfires emit large amounts of primary pollutants, like black carbon (BC), carbon monoxide

64   (CO), nitrogen oxides ($NO_x=NO+NO_2$), and volatile organic compounds (VOCs). Studies of

65   boreal fire emission show that the NO_x concentration is doubled , and BC increases by 10 times

66   during the wildfire period (Val Martín et al., 2006). Previous studies indicate that NO_x and VOCs

67   emissions from wildfires have influences on the O_3 budgets, the enhancement of O_3 ranging from

68   5 to 20 ppb on average (Val Martín et al., 2006; Baylon et al., 2015; McClure et al., 2018;

69   Buysse et al., 2019). When wildfire smoke reaches urban regions, the NO_x, and VOCs from

70   wildfire smoke is believed to enhance O_3 production (Akagi et al., 2013; Singh et al., 2012) and

71   exacerbate the already problematic ozone pollution levels in urban areas. Brey and Fischer (2016)

72   found that the mean O_3 abundance measured on smoke-impacted days is higher than smoke-free

73   days and the magnitude varies by location with a range of 3 to 36 ppbv. But most importantly,

74   they also found that the smoke-impacted O_3 mixing ratio are most elevated in locations with the

75   highest emissions of nitrogen oxides.

76   However, the O_3 response could vary from significant enhancement to small enhancement and

77   even depletion during different wildfire events (Val Martín et al., 2006). McClure et al. (2018)

78   and Buysse et al. (2019) also report that MDA8 O_3 tend to decrease during heavy smoke

79   influenced period when $PM_{2.5}$ exceeds 70 μg/m^3. The reasons for this are not fully understood

80   but may be explained by some of the following conjectures in the literature. Alvarado et al.

81   (2015) found that on average 40 percent of the NO_x was converted to *peroxyacetyl nitrate* (PAN)

82   within 1-2 hours after emission. The decomposition of PAN at downwind locations during

83   adiabatic warming by subsidence could be attributed to about 8 ppb out of 20 ppb of O_3

84   enhancement (Fischer et al., 2010). The loss of O_3 by reaction with organic carbon could also

85   decrease O_3 concentration in wildfire plumes. de Gouw and Lovejoy (1998) found that

86   heterogeneous reaction between O_3 and organic aerosol can be an important loss for tropospheric

87   ozone if aerosol contains unsaturated organic material. Apart from that, Buysee et al. (2019)

88   found lower NO/NO_2 ratio when the sites are influenced by wildfire smoke and provided several

89   potential reasons like elevated atmospheric oxidants, higher temperature, lower rates of NO_2

90   photolysis. Moreover, huge amounts of aerosol particles like organic carbon and black carbon

91   emitted from biomass burning could influence the amount of radiation that reaches the surface.

92   Airborne studies using aerosol and radiation measurements indicate that a layer of high

93   concentration of aerosol is sometimes detected just below the temperature inversion, which

94   hinders the vertical exchange, and could drastically reduce the downwelling solar and UV

95   irradiance, as well as the surface $j(NO_2)$ (Wendisch et al., 1996). Baylon et al. (2018)

96   implemented research about wildfire impacts on ozone production at a high elevation site located

97   on Mt. Bachelor, and reported $j(NO_2)$ decreases of 14 to 21% at high solar zenith angle when

98   biomass burning plumes were detected, but slight increases (0.2~1.8%) of $j(NO_2)$ were found at

99   local noon. Since O_3 production depends on actinic radiation, the wildfire smoke shading on NO_2

100   photolysis needs to be considered. Furthermore, the meteorological factors, such as temperature

101   and humidity could also affect the reaction associated with O_3 production (Lin et al., 2017;

102   Zhang et al., 2014). One study of the temperature dependence of ozone production in the San

103   Joaquin Valley (SJV) (Pusede et al., 2014) found that the reactivity of total volatile organic

104   compound with OH (VOCR) (s^{-1}), summed HO_x production rate (PHO_x $ppts^{-1}$) increases

105   exponentially with temperature while NO/NO_x decreases resulting in higher midday O_3

106   concentration. A recent model simulation study of a 2013 California wildfire did well at

107   capturing near-fire smoke plume transport based on satellite and aircraft measurements (Baker et

108   al., 2018). Although the photolysis rates in that study were also found to be well characterized by

109   the model, the predicted O_3 was not well aligned with surface site or aircraft measurements: O_3

110   tends to be overestimated both aloft and at the surface when the model predicts impacts from

5

111   wildfire. In the United States, the current ozone standard of National Ambient Air Quality

112   Standard (NAAQS) is 70 ppb for an 8-hour average. According to California Air Resource

113   Board (CARB), ozone concentrations are frequently exceeding existing health-protective

114   standard in metropolitan areas of California during summertime. In addition, the southern part of

115   California's Central Valley, San Joaquin Valley, is still one of the two extreme ozone

116   nonattainment area remaining in the U.S. (U.S. EPA Green Book, www.epa.gov/green-book).

117   With the projection of increasing likelihood of large wildfire in the future across the western U.S.

118   (Stavros et al, 2014), it is important to understand the yet uncertain mechanism of ozone

119   production during wildfire events in California's Central Valley (CV).

120   In addition to the pollutants from wildfire, previous studies indicate that the shading effect of

121   wildfire smoke can decrease the surface heat fluxes and the convective activity within the ABL

122   (Pahlow et al., 2005). Pal and Haeffelin (2015) implemented a 5-year observational study of

123   ABL height and other related variables near Paris in which they found the strongest determinant

124   (r=0.92) of daily maximum ABL height was downwelling shortwave radiation (SSWD). Daily

125   maximum ABL height and surface sensible heat flux (Q_H) are also found to be correlated (r=0.75)

126   but not as strongly. That SSWD is found to be most correlated to maximum ABL height was

127   further verified by Trousdell et al. (2016) in the SJV. The lowest portion of free troposphere (FT)

128   in San Joaquin Valley (SJV) has a complex structure with a 'buffer layer' residing between ABL

129   and FT, which is a layer of relatively stagnant air at altitudes between 500m to 2500m, resulting

130   from the onshore wind that impinges on the Southern Sierra Nevada mountains on the east side

131   of SJV (Faloona et al., 2020). This 'buffer layer' accumulates the pollutants from the ABL by

132   anabatic sidewall venting during the daytime but continuously returns some of the air via midday

133   entrainment, and turbulence within the ABL is the key factor that controls the entrainment

134   process. Thus, studying the wildfire impact on ABL height and its turbulence activity will shed

135   more light on the ventilation process of pollutants in SJV.

136   In this paper, we use the data from 10 CARB monitoring sites in California's Central Valley

137   to quantify the impact of wildfire smoke during summer (Jun-Sep) from 2016 to 2020. Then, we

138   use measured O_3, NO and NO_2 mixing ratio with the modified Leighton relationship (Volz-

139   Thomas   et al., 2007) to calculate ozone production rate $P(O_3)$, where we also account for the

140   shading effect of the wildfire smoke on $j(NO_2)$, variation in ambient O_3, and k_{O_3} (rate constant

141   in reaction 2) changes due to temperature variations. We also present the enhancement ratios

142   (ERs) of $PM_{2.5}/CO$, O_3/CO, $O_3/PM_{2.5}$, and ozone production efficiency (OPE) in order to

143   characterize the pollutant emission ratios from the wildfire plumes in the Central Valley. Then,

144   we discuss the influences of wildfire smoke on surface fluxes ($\overline{w'\theta_v'}$, Q_H, and Q_E) measured by

145   two AmeriFlux monitoring sites located in the northern part of SJV. Besides, we also use radio

146   acoustic sounding system (RASS) locate near Visalia to study wildfire impacts on temperature

147   profile and ABL height. Our study aims at inferring the causal relationships to water vapor

148   dynamics, boundary layer heights, and entrainment rates.

149   **2. Data and Methods**

150   *2.1.   Measurements*

151   Measurements of hourly $PM_{2.5}$, O_3, nitric oxide (NO), nitrogen dioxide (NO_2), and CO are

152   from 10 monitoring sites in California's Central Valley (CARB). Meteorological data, such as

153   temperature, dew point, and pressure are obtained from the airport located near each air pollution

154   monitoring site .The locations and other detail information of the sites can be found in Table 1.

155   All the air pollution and meteorological data are download via California Air Resources Board

156   (CARB), except for the data of reactive nitrogen compounds (NO_y) are downloaded via <u>AirNow-</u>

157   <u>Tech</u>. The missing hourly measurements are replaced by averaging of the hour before and after,

158   otherwise the missing points are abandoned. We have removed 0.81% of negative measurements

159   of hourly $PM_{2.5}$. We use temperature and relative humidity data from the monitoring sites of

160   CARB if they are available, otherwise we use the variables measured from the meteorological

161   sites at the nearest airport. Since relative humidity is a function that strongly depends on

162   temperature, we also calculate specific humidity (q) from pressure measurements and the

163   Clausius-Clapeyron relationship at the airport to eliminate the direct dependence on temperature.

164   Because approximately 80% of ozone exceedance days in the SJV typically occur between June

165   1 and September 30 (Trousdell et al., 2019), we focus on this period for each year. We calculate

166   24-hr $PM_{2.5}$ and MDA O_3 as daily metrics, and the average of other pollutant concentrations

167   from 10:00 and 15:00 PST as daytime averages.

168   The conventional measurement of NO_2 entails the catalytic conversion from NO_2 to NO on a

169   heated molybdenum surface and subsequently measured by chemiluminescence after reaction

170   with ozone. The drawback of this method is that other oxidized nitrogen compounds such as

171   PAN and HNO_3 can also be converted to NO, thus NO_2 chemiluminescence measurements are

172   generally overestimated. Steinbacher et al. (2007) proposed a correction method for

173   overestimated NO_2 measurements based on their long-term observations in Switzerland in

174   Equation (6):

$$\Delta NO_2 = a \cdot (NO_2)_m + b \cdot O_3 + c \cdot f(month) + d \cdot f(day) + e + \varepsilon \qquad (6)$$

175   Where ΔNO_2 is the amount of overestimation for NO_2, $(NO_2)_m$ is the measured NO_2

176   concentration, O_3 is measured ozone concentration. a, b, c, d, e, and $f(month)$ are constants,

177   and $f(day)$ is binary predictor distinguishing day time and night time (1 or 0) , and ε is the

178 residual term that we ignored in our study. Details about those constants could be found in Table

179 S1. All the NO_2 measurements in this study are corrected according to Equation (6).

180 *2.2.   Wildfire identification*

181   We use Hazard Mapping System (HMS) accessed from AirNow-Tech as an indicator of

182 wildfire events. HMS detects fire locations and digitizes smoke plume areal extent by combining

183 polar and geostationary satellite observations and creating a map for North America around 7-8

184 a.m. (PST) daily. For the time zone of the CV, the site may not detect overhead smoke by HMS

185 in the morning but could be affected by smoke for rest of the day. Besides, the HMS system is

186 observed from above, therefore it will not differentiate surface wildfire plumes and the plumes

187 aloft and may also be limited by any cloud cover. These limitations may cause improper

188 identification of wildfire events thus we need additional methods to verify the presence of

189 ground level smoke. The Hybrid Single Particle Lagrangian Integrated Trajectory model

190 (HYSPLIT) was used to analyze the back-trajectory of the air parcel at each target site and

191 decide its origin at ground level. By using HMS and HYSPLIT, the wildfire identification steps

192 are as follow: First, we use the HMS product to see if any sites are covered with smoke, the

193 target sites are marked according to category of HMS product as thin, medium, and thick smoke

194 coverage. Second, we use HYSPLIT model to calculate 24-hour back-trajectories at 12:00 P.M.

195 PST for each site with HMS overhead wildfire cover of any magnitude. The model is performed

196 at altitudes of 100m, 600m and 1500m, respectively, which will provide the transport pattern

197 near the surface, the top of boundary layer and in the middle of "buffer layer" (Faloona et al.,

198 2020) or sometimes called the "stable core layer" (Leukauf et al., 2016) of a valley atmosphere.

199 If both of the HMS shows overhead smoke and one of the HYSPLIT back-trajectory is

200 originated from the vicinity area of fire point, we define the target site at that day as influenced

201   by wildfire smoke. Moreover, we also mark the wildfire days with HMS showing overhead

202   smoke but HYSPLIT not indicating lower-level smoke transport. The background values are

203   obtained from the data of the sunny days, which are identified by visualizing the cloud coverage

204   from true color reflectance of MODIES Aqua and Terra.

205   *2.3.   Ozone production*

206   The modified Leighton relationship is a method to determine the relative magnitude of the in-

207   situ photochemical ozone production rate by measuring the extent to which the O_3-NO_x cycle is

208   away from the photostationary state. This method represents the photochemical cycle of O_3, NO_x,

209   HO_2 and RO_2 (Leighton, 1961).

$$\frac{[NO]}{[NO_2]} = \frac{j(NO_2)}{k_{O_3}[O_3] + k_{HO_2}[HO_2] + k_{RO_2}[RO_2]} \qquad (7)$$

210   The chemical reactions entailed in this cycle are in Equation (1)-(4), where $j(NO_2)$ is the

211   photolysis rate in reaction (1), k_{O_3}, k_{HO_2} and k_{RO_2} are rate constant for reaction (2), (3) and (4).

212   The role of wildfire smoke will include the additional NO_x and VOCs, which result in changing

213   the concentration of HO_2 , RO_2, NO_x and its ensuing effect on O_3 production.

214   The ozone production rate is derived from modified Leighton relationship from Equation (7).

215   Reactions (3) and (4) determine the limiting rates for ozone production, thus the production rate

216   of NO_2 in (3) and (4) is the effective production rate for 'new' O_3 that does not belong to the

217   instantaneous photostationary state .This can be expressed as:

$$P(O_3) = [NO]\{k_{HO_2}[HO_2] + k_{RO_2}[RO_2]\} = j(NO_2)[NO_2] - k_{O_3}[O_3][NO] \qquad (8)$$

218   where [NO], [NO$_2$] and [O$_3$] are hourly averaged mixing ratio measured by CARB, and

219    $k_{HO_2}[HO_2] + k_{RO_2}[RO_2]$ represent the contribution of VOC in ozone production. The direct

220   measurements of $j(NO_2)$ at ground level are often not available in field studies. Trebs et al.

221   (2009) reported a relationship that can be used to estimate ground-level $j(NO_2)$ directly from the

222   solar irradiance, which is nowadays measured as a standard parameter in most field

223   measurements. In order to account for the shading effect on $j(NO_2)$ from wildfire smoke, we use

224   solar radiation measurements from California Irrigation Management Information System

225   (CIMIS) to calculate the average daily profile at each site during non-fire days for each month,

226   then we use the ratio of the radiation profile for a fire day divided by the monthly averaged non-

227   fire day profile to obtain the amount of attenuation from the smoke plume. Eventually, we use

228   the tropospheric ultraviolet (TUV) calculator accessed from Atmospheric Chemistry &

229   Modelling from National Center for Atmospheric Research (NCAR) to calculate the hourly

230   averaged $j(NO_2)$ profile for non-fire day, and using the attenuated solar radiation during the

231   wildfire influenced period to scale the $j(NO_2)$. This approach is employed to account for the

232   decreased photolysis rate during wildfire events due to the shading effect of smoke. Note that in

233   Trebs et al. (2009) study, they use a second-order polynomial function to calculate $j(NO_2)$

234   directly from surface irradiance, whereas our study uses a simple linear scaling of downwelling

235   short wave to simulate the change of $j(NO_2)$. Since we only focus on the relative changes of

236   surface radiation and $j(NO_2)$ during midday between fire and non-fire, thus the zenith angles are

237   low enough to not be influenced by more challenging scatter effects that might arise at higher

238   solar zenith angles. Moreover, k_{O_3} is also adjusted to corresponding hourly-averaged temperature

239   measured at each site to account for the changes of rate constant due to temperature change.

$$k_{O_3} = 3.47 \exp\left(-\frac{1533}{T}\right) \ cm^3/molecule \quad (9)$$

240   Equation (9) is the Arrhenius function to calculate k_{O_3} based on temperature T, the rate

241   expression fits experiment result extremely well through the common temperature range of 283-

242   364K. (Lippmann et al., 1980)

243   The concentration of HO_2 and RO_2 is estimated from Equation (8). Although the HO_2 and

244   RO_2 tend to be overestimated by using this method (Griffin et al., 2007; Volz-Thomas et al.,

245   2003; Mannschreck et al., 2002), it is still useful when we compare the estimated HO_2 and RO_2

246   between wildfire influenced periods and background periods in order to investigate the impact of

247   additional VOC on ozone production. Where the rate constant of reaction (5) and (6) is expressed

248   by another Arrhenius function $k = A exp(-E_a R/T)$ (Brasseur et al., 1999), where T is

249   temperature in Kelvin. The details of factor A and constant $-E_a R$ are in supporting information

250   (Table S2). We consider the sum of HO_2 and RO_2 as RO_x for the reaction and they are calculated

251   by Equation (7) by the method in Baylon et al. (2018).

252   *2.4.   Boundary layer dynamics*

253   We use surface flux data from two AmeriFlux sites located at Twitchell Wetland (Valach et

254   al., 2012) (38.1074 N, 121.6469 W, -5m) and Vaira Ranch (Baldocchi et al., 2000) (38.4133 N,

255   120.9507 W, 129m), respectively. The Twitchell site has a flux tower equipped to analyze

256   energy, H_2O, CO_2, and CH_4 fluxes since May 2012, which is located at a 7.4-acre restored

257   wetland on Twitchell Island. The wetland is almost completely covered by cattails and tules by

258   the third growing season. Vaira Ranch site has been established at the lower foothills of the

259   Sierra Nevada mountains on privately owned land since 2000, the site is classified as a grassland

260   dominated by C3 annual grasses. The measurements at two sites include surface sensible heat

261   flux (Q_H), latent heat flux (Q_E), temperature, incoming shortwave radiation, and the mole

262   fraction of water vapor. The time resolution is 30 minutes, and the measurements are available

263   from 2016 to 2019. The surface buoyancy flux is calculated by Equation (8), where $\bar{\theta}$, $\overline{w'\theta'}$ and

264    $\overline{w'q'}$ are direct measurement from the site, $\bar{q}$ is calculated from the measured mole fraction of

265   water vapor.

$$\overline{w'\theta'_v} \cong \overline{w'\theta'}(1 + 0.61\bar{q}) + 0.61\bar{\theta}\,\overline{w'q'} \qquad (10)$$

266   We use the same wildfire events identification results from section 2.2 of chapter 1 to

267   categorize wildfire days and background days, where Twitchell Island (30km northwest of

268   Stockton) uses the results of Stockton and Vaira Ranch (50 km southeast of Sacramento) uses the

269   result of Sacramento. Then, we calculate the average daily profile for $\overline{w'\theta'_v}$, Q_H, Q_E, and

270   incoming shortwave radiation for wildfire influenced days and sunny days at each site.

271   Radio acoustic sounding system (RASS) can remotely measure the virtual temperature and

272   wind profile up to 2km, and its 1-hour time resolution has substantial advantage over

273   radiosondes. We use the virtue temperature data measured by RASS located near Visalia

274   Municipal Airport. Then, the virtual temperature is converted into virtual potential temperature

275   by the hypsometric and Poisson's equations based on the surface measurements of temperature

276   and pressure. The ABL height is estimated by the first range gate where the vertical virtual

277   potential temperature gradient exceeds 10 K/km. Then, the estimated ABL heights are also

278   sorted into wildfire influenced days and sunny days for comparison. A 5-year monthly averaged

279   diurnal ABL height profile retrieved by this method during June to September, 2016-2020 is

280   shown in Figure S5. The magnitude and timing of the ABL heights match the diurnal ABL

281   depths in SJV measured by Bianco et al. (2011) and Faloona et al. (2020).

282   **3.   Results and Discussion**

283   *3.1.   Summary of wildfire events from 2016 to 2020*

284   During the summer time (June to September) in California's Central Valley, wildfires are

285   prone to happen along the mountain ridges that surround the valley. The yearly acres burned by

286   wildfire in California ranging from 259,148 in 2019 to 1,823,153 in 2018 (National Interagency

287   Coordination Center). By 06 September 2020, the 2020 fire season in California has become the

288   most intense year of the 18-year long fire radiative power measurement from satellite data

289   (NOAA/NESDIS Hazard Mapping System). Figure 2 shows a snap shot of HMS product at

290   12:00 PST 23 September 2020 accessed from AirNow-Tech. Fire locations are marked with red

291   triangles and HMS smoke coverage is denoted by shading area with different gray scales depend

292   on the intensity of the smoke. In this snapshot, the entire CV is covered with smoke from the top-

293   down view. However, the HYSLPIT model performed at Fresno shows the air parcel was from

294   Pacific Ocean through the San Francisco Bay Area and reached its destination, which means the

295   air near ground level and at ABL top had likely not originated nor passed near the vicinity area

296   of the wildfire source, despite its proximity to Fresno. The ground level 24-hr $PM_{2.5}$ at Fresno-

297   Garland confirmed it with a measurement of only 9.1 $\mu g/m^3$. This is a typical case in which HMS

298   shows an overhead smoke plume but the ground level is not affected by wildfire emissions.

299   Although the wildfire influenced periods vary from site to site, the total number of wildfire

300   influenced days are about 120 days out of 600 days (~20%) from our 5-year data analysis.

301   We summarize the characteristic value of daily maximum temperature (T_{max}), relative

302   humidity (RH), specific humidity (q), scalar-mean windspeed (u), 24-hr $PM_{2.5}$, MDA8 O_3, CO

303   and NO_x for wildfire days and none-fire days at each site in Figure 3. The error bars show inner

304   quartile limited by 25th and 75th percentiles, and the center mark denotes the median value. For

305   24-hr $PM_{2.5}$ and CO, concentrations on wildfire days are significantly higher than non-fire days

306   at all sites, since fine particles and CO are major products of biomass burning and are also good

307   tracers for wildfire effluent. Note that the 25th percentile of wildfire value is comparable or even

308   higher than the 75th percentile of non-fire period, which suggests that using background $PM_{2.5}$ or

309   CO as a threshold for ground level wildfire identification as has been done in previous studies

310   (McClure et al., 2018; Briggs et al.,2016) is a decent identification method that does not require

311   using the HYSPLIT model. The MDA8 O_3 and NO_x concentrations also have a noticeable

312   enhancement during fire days, suggesting that wildfire plume indeed provide additional NO_x

313   causing an enhancement in O_3 concentration. The histograms in Figure S1 also show that almost

314   28% of the wildfire influenced days exceed the NAAQS of 70 ppb MDA8 O_3 versus only 12%

315   during background periods. Besides, the MDA8 O_3 also show a geographical bias, with higher

316   O_3 concentration in the SJV than in the SV regardless of whether or not wildfire emissions are

317   present. This result is consistent with the EPA Green Book and the study conducted by Trousdell

318   et al. (2019), in which they state that ozone pollution in the SJV is still a problematic issue.

319   For meteorological factors, all sites except Chico show a higher median value (~0.5K on

320   average) of daily maximum temperature (T_{max}) on wildfire influenced days, though the median

321   T_{max} is lower at Chico during wildfire period. This result matches the previous long-term

322   climatology studies on wildfire in Canada during 1953 to 1980 (Flannigan and Harrington, 1987)

323   and in U.S. from 1971 through 1984 (Potter, 1996), in which they report that wildfire events

324   correspond to positive temperature anomalies. However, a surprisingly consistent higher specific

325   humidity (q) is observed at all sites during wildfire periods by 0.6 g/kg on average. In addition,

326   higher RH values are also detected at most sites except for Merced and Bakersfield. The increase

327   in water vapor content during wildfire influence is somewhat counterintuitive and does not align

328   with previous studies (Flannigan and Harrington, 1987; Potter, 1996) since wildfires are more

329   likely to occur on days with low humidity. Furthermore, the windspeeds show a reduction of

330   about 0.5 m/s on average during wildfire periods at most sites except for Madera and Fresno.

331   Again, this result runs counter to previous studies (Bryam et al., 1954; Rothermel et al., 1991), in

332   which they suggest that stronger winds often play a role in spearing crown fires. The typical

333   meteorological conditions favorable for wildfire would thus be higher temperatures and

334   windspeed combined with lower relative humidity. Our results exhibit differences in windspeed

335   and RH, which denote that the lower windspeed and higher RH could be due to other factors. We

336   hypothesize that the higher water vapor content and lower wind speeds are the result of weaker

337   ABL entrainment due to the shading effect from wildfire plumes because of the reduced surface

338   heat fluxes. This will be discussed more in section 3 of chapter 2.

339   In order to characterize the pollutant emission ratios from the wildfire plumes, multiple

340   enhancement ratios (ERs) are indicated at each site in Figure 4. All the enhancements are the

341   differences between the median value of daytime averages (10:00-15:00 PST) on wildfire days

342   vs. non-fire days. $\Delta O_3/\Delta T_{max}$ in Figure 4a represent the enhancement of MDA8 O_3 with respect

343   to change in maximum temperature. The relatively strong correlation (r^2=0.513) with a slope (i.e.

344   m value) of 3.73 ppb/K indicates that the observed ozone enhancements are partially the result of

345   temperature differences. Furthermore, the zero crossing of the regression in Figure 4a (ΔT_{max}=0)

346   is about 5ppb, which means that without any observed temperature difference, the ozone

347   concentrations are enhanced from the wildfires by about 5ppb across the CV. According to

348   Pusede et al., 2014, a study of daily maximum temperature versus day time (10:00-14:00 LT) O_3

349   concentration in Bakersfield shows that $\Delta O_3/\Delta T_{max}$ is around 2 ppb/K. And Steiner et al. (2010)

350   report ozone-temperature slopes of 2.4 ppb/K and 1.8 ppb/K in SJV and SV, respectively, yet

351   their data is already a decade old and they found that these slopes were decreasing over the 30

352   years of their study. Our study (Figure S2) shows that $\Delta O_3/\Delta T_{max}$ is 1.7 ppb/K for the

353   background periods in SJV and 1.3 ppb/K in the SV consistent with a continued decrease in this

354   parameter. Moreover, we found that the average slopes increase in the presence of wildfire

355   emissions to 2.2 ppb/k (SJV) and 1.6 ppb/K (SV) also consistent with its dependence on

356   precursor emissions (Sillman & Sampson, 1995). Thus, with an average of 0.5 K increase in

357   temperature, we expect that approximately 0.8 ppb of the observed O_3 enhancement is due to the

358   average temperature difference during wildfire periods and another 0.2 ppb is due to the shift in

359   chemical regime. We use CO and $PM_{2.5}$ as a tracer for wildfire smoke since they are major

360   products of biomass burning. We characterized the enhancement of MDA8 O_3 with respect ΔCO

361   and $\Delta PM_{2.5}$ to quantify the O_3 enhancement due to the wildfire smoke. Figure 4b shows

362    $\Delta O_3/\Delta PM_{2.5}$ respect to their temperature change (ΔT_{max}) at each site, which also have a relatively

363   strong correlation (r^2=0.588) and the ratios increase with temperature and the zero cross

364   (ΔT_{max}=0) is about 0.5 ppb/μgm^{-3}. The $\Delta O_3/\Delta PM_{2.5}$ in Figure 4c increase from north to south

365   (r^2=0.588) as well as ratios for $\Delta O_3/\Delta CO$ at each site showed in Figure S3b (r^2=0.237), the

366   possible explanation for this could be the strong influences of temperature on ozone

367   concentration (Figure S2) and the higher temperature enhancement in SJV (Figure 4d), where the

368   ΔT_{max} and the latitude have a r^2 value of 0.824. Our values for $\Delta O_3/\Delta PM_{2.5}$ and $\Delta O_3/\Delta CO$ are

369   ranging from 0.2 to 1.4 ppb/μgm^{-3} and 0.04 to 0.14 ppb/ppb, respectively, which are within the

370   ranges reported in the literature (Val Martín et al., 2006; Baylon et al.,2015; McClue et al., 2018).

371   Note that $\Delta O_3/\Delta CO$ ratios are an indicator of plume age, where higher ratios tend to represent

372   greater plume ages (Jaffe and Wigder et al., 2012). Our ratios of $\Delta O_3/\Delta CO$ are similar to the

373   values reported in Alvarado et al. (2010) and Yokelson et al. (2009), where the plume age is

374   within several hours, and our observed average ratio of 0.05 is very similar to the average

375   reported in Baylon et al. (2015) for plumes between 12 and 24 hours old. We also found that the

376   ERs of $\Delta PM_{2.5}/\Delta CO$ have a strong positive correlation among all ten sites (Figure S4), indicating

377   that the $PM_{2.5}$ and CO are well connected to wildfire influence. Our average ER for $\Delta PM_{2.5}/\Delta CO$

378   (m value in Figure S4) is 0.13 ($\pm$0.02) μg/m^3 ppb^{-1}, which agrees well with the value found by

379   Selimovic et al. (2019) in a study from two summers in Montana as well as the value reported by

380   McClue and Jaffe (2018) from fires in Idaho. Wildfire smoke influences on PM and ozone

381   production

382   In order to investigate the O_3 variations and their relationship to the existence of additional

383   PM from wildfire smoke, we plot the binned 24-hr $PM_{2.5}$ versus corresponding MDA8 O_3 in

384   Figure 5a. Since O_3 enhancement reacts differently across the CV, we separate our sites into two

385   geographical categories: Chico, Yuba City and Sacramento into Sacramento Valley (SV) (Figure

386   5b) and other sites into SJV (Figure 5c). Generally, MDA8 O_3 increases with PM at low 24-hr

387    $PM_{2.5}$ concentration for both of the wildfire and background periods, peaking around 40 to 55 µg

388   /m^3, then becomes independent of PM at higher concentration ($PM_{2.5}$ >55 µg /m^3). The slope

389   rates of O_3 to $PM_{2.5}$ are higher in the SJV than the SV, which is consist with the result of higher

390    $\Delta O_3/\Delta PM_{2.5}$ in section 3.1. The non-linear relationship in our results generally aligns with the

391   results from previous studies (McClure et al., 2018; Buysse et al.,2019), in which an increase of

392   MDA8 O_3 with PM was found at low to moderate PM with a peak of MDA8 O_3 around 40 to 55

393   µg/m^3. However, our results do not show a clear decreasing trend of MDA8 O_3 at higher PM.

394   The MDA8 O_3 did slightly decrease when $PM_{2.5}$ exceed 55 µg /m^3 in SJV, but it returns to its

395   peak value when $PM_{2.5}$>100 µg /m^3. Besides, the MDA8 O_3 when PM> 100 µg /m^3 in SV is

396   actually higher than its value around 40 to 55 µg /m^3. Thus, our results suggest that MDA8 O_3

397   starts to increase again with $PM_{2.5}$ when it exceeds 100 µg /m^3.

398   The O_3 production rate (PO_3), concentration of peroxyl radical (RO_2+HO_2), NO, and

399   attenuation of incoming solar radiation are shown in Figure 6. The peak value of solar radiation

400   (Figure 6d) decreases by 7% on average at all ten sites during wildfire periods, which will

401   approximately scale to approximately the same amount of $j(NO_2)$ attenuation. The PO_3 (Figure

402   6c) that is calculated from the modified Leighton ratio increases at all sites during the wildfire

403   influenced periods, despite the diminution of $j(NO_2)$ due to the shading effect of wildfire smoke.

404   The PO_3 increases more in SJV by 37% than in SV by 24%. The higher PO_3 enhancement in SJV

405   is consistent with the result of higher $\Delta O_3/\Delta PM_{2.5}$ and $\Delta O_3/\Delta CO$ in section 3.1. This also

406   suggests that O_3 production is more sensitive to the presence of wildfire smoke in SJV than SV.

407   The concentration RO_2+HO_2 (Figure 6b) does not show a uniform pattern among all ten sites.

408   Sacramento, Stockton, Merced, Fresno, and Bakersfield show prominent enhancement in

409   RO_2+HO_2 concentration, whereas only Stockton and Fresno detect enhancement in NO (Figure

410   6a) concentration. However, despite the insignificant increment of NO, all sites have an

411   enhancement of in-situ PO_3, which implies that the role of wildfire smoke is to provide

412   additional RO_2 and HO_2 to the O_3 photolysis cycle. Note that in Madera and Visalia, the opposite

413   situation occurs, where NO has higher concentration during wildfire periods but RO_2+HO_2

414   concentrations have negative increment. This phenomenon may suggest that without the

415   presence of additional RO_2 and HO_2, the additional NO from the wildfire plume alone could

416   also increase in O_3 production. The PO_3 and RO_2+HO_2 concentrations that are estimated from

417   the modified Leighton ratio in our study tend to be much higher than measured or modeled

418   values (Pusede et al., 2014; Tan et al., 2018). Volz-Thomas et al. (2003) also used Leighton ratio

419   to estimate PO_3 and the result yields up to 90 ppb/h, which is similar to the magnitude of our

420   result at some sites. They also calculate PO_3 from measured peroxyl radical and the result was

421   much lower, around 10 ppb/h. Despite our result showing prominent differences of PO_3 between

422   wildfire and background periods, we suspect that the overestimation of PO_3 is due to the

423   inaccurate estimation of peroxyl radiation based on Leighton ratios. Hence, a yet unknown

424   process must exist in tropospheric O_3 production that converts NO to NO_2 without leading to a

425   net production of O_3. Nevertheless, we believe that the relative changes in $P(O_3)$ and $[HO_2]$ +

426    $[RO_2]$ are still instructive. Across the CV the average $P(O_3)$ increases by about 35% under the

427   influence of wildfires, with approximately two-thirds of that increase due to elevated $[HO_2]$ +

428    $[RO_2]$ and one-third due to elevated NO, implying that the wildfire smoke enhances ozone by

429   increasing oxidized VOCs by about twice as much as it increases NO_x.

430   Ozone production efficiency (OPE) is defined as the enhancement of O_x (O_3+NO_2) with

431   respect to NO_z (NO_y-NO_x). It describes the amount of O_3 that is produced per NO_x molecule

432   consumed (Liu et al., 1987; Lin et al., 1988; Trainer et al., 1993; Olszyna et al., 1994). Figure 7

433   shows scatter plots for O_x vs. NO_z at Sacramento and Fresno during the 2016-2020 ozone

434   seasons for wildfire and clear-sky data. The slope value (m) is the enhancement of O_x with

435   respect to NO_z, or OPE. The OPE for Sacramento and Fresno during wildfire influenced periods

436   are 4.4 and 8.3, respectively. The y-intercept of O_x-NO_z plot (b value) represent the background

437   ozone. The observations of 19 fire plumes at Mt. Bachelor show OPE ranging from 2.1 to 17

438   (Baylon et al., 2015). The higher OPE value in Fresno could be due to the higher temperature in

439   SJV than SV (Figure 2), since the temperature dependence is associated with the decomposition

440   rate of PAN (Sillman and Samson, 1995). Pusede et al. (2014) found that the O_3 production in

441   SJV is NO_x-limited during summer, most notably at higher temperatures. Because the NO_x levels

442   are comparable in the two valleys, the greater OPE in the SJV implies a correspondingly greater

443   VOC/NO_x ratio, and therefore generally more NO_x-limited conditions than in the SV. More

444   importantly, the OPE during wildfire periods are both ~1 ppb O_x/ppb NO_z higher than in the non-

445   fire periods, which are 3.1 and 7.3 for Sacramento and Fresno, respectively. The increased OPE

446   at both sites further indicates that smoke plumes provide more VOCs than NO_x (increase the

20

447   VOC/NO$_x$ ratio) so that the conditions incline to be slightly more NO$_x$-limited when influenced

448   by wildfires.

449   *3.2.*   *Wildfire smoke influence on boundary layer dynamics*

450   Measurements of surface heat fluxes (Q_H, Q_E, and $\overline{w'\theta_v'}$) and incoming shortwave radiation

451   (SSWD) at Twitchell Wetland (bottom) and Vaira Ranch (top) are shown in Figure 8. Both of

452   the sensible heat flux Q_H and buoyancy flux $\overline{w'\theta_v'}$ decrease during the wildfire periods,

453   especially for Twitchell Wetland, where $\overline{w'\theta_v'}$ and Q_H are only 50% of its magnitude on sunny

454   days. The peak value of Q_E at Vaira Ranch decreases by 20 W/m^2 but increases by 20% on

455   average at Twitchell Wetland. Note that, due to the difference in land types, the moisture is

456   significantly higher in Twitchell than Varia, which explains the significantly smaller Q_E in Vaira

457   Ranch compared to Twitchell Wetland with a Bowen ratio of 11.7 and 0.6, respectively. The

458   reduced SSWD , Q_H, and $\overline{w'\theta_v'}$ will weaken the turbulence mixing within ABL and reduce the

459   ABL height, which in principle could enhance the specific humidity and weaken the surface

460   wind speed since a reduced buoyancy source of turbulent kinetic energy (TKE) will reduce the

461   entrainment fluxes of dry, higher momentum air across the inversion. Our results are consistent

462   with the LES study of aerosol loading in the ABL by Liu et al. (2019), which showed that as

463   aerosol optical depth (AOD) increases, less solar radiation reaches the surface, reducing the

464   surface buoyancy flux, and weakening the entrainment.

465   Figure 9a is the profile of virtual potential temperature (θ_v) measured by the RASS located in

466   Visalia. The profile is averaged from 13:00 to 15:00 PST during summer 2016-2020 for wildfire

467   days (red) and sunny days (black), respectively, since daily maximum ABL height usually occurs

468   around 14:00 in SJV (Bianco et al., 2011). The θ_v at the surface during wildfire days is about 1.5

469   K higher than non-fire days, which is consistent with our result in section 3.1 of chapter 1 where

21

470   the daily maximum temperature at most sites are higher during wildfire period. Furthermore, θ_v

471   within the entire ABL, and in fact well above it, is also consistently higher during wildfire days,

472   which implies that aerosol within the lower valley atmosphere from wildfire plumes absorb solar

473   radiation and warm the ABL and buffer layer. Liu et al. (2019) also simulated a warmer ABL

474   when aerosols were present in their LES model, and the potential temperature increases with

475   higher AOD. A 5-year averaged diurnal ABL height comparison between wildfire periods and

476   background days are shown in Figure 9b, with SSWD comparison shown in Figure 9c. The

477   midday ABL height (Figure 10b) is reduced by 80 m and the SSWD by about 54 W/m^2, on

478   average. Pal and Haeffelin (2015) reported the slope for SSWD versus daily maximum ABL

479   height to be 1.73 m/Wm^{-2} from an observatory outside of Paris, and Trousdell et al. (2016) report

480   a similar slope of 1.51 m/Wm^{-2} in the SJV. The observed reduction in ABL height due to the

481   wildfire shading effects shown in Figure 9 are quantitatively consistent with these other findings

482   (80 m/54 Wm^{-2} = 1.48 m/Wm^{-2}).

483   Thus, wildfire smoke has two roles in influencing the ABL dynamics: first, by attenuating the

484   solar radiation that reaches the surface it reduces the surface heat fluxes weakening entrainment

485   thereby decreasing the maximum ABL height, and second, it absorbs solar radiation warming the

486   air in the ABL (and above) thereby offsetting the reduced surface heat fluxes in terms of its

487   impact on air temperature. Figure S6 present the backscatter profile from Tunable Optical

488   Profiler for Aerosol and Ozone lidar (TOPAZ) observed during the June – August observed

489   during the California Baseline Ozone Transport Study (Langford et al., 2020; Faloona et al.,

490   2020). The backscatter is seen to be much stronger in ABL, and to a lesser extent above (up to

491   about 2,500 m), during the wildfire periods (left) compared to the background days (right). Since

492   the wildfire plumes will weaken the entrainment at ABL top and lower the ABL height, the rate

493   of dilution from the buffer layer into the ABL and volume for pollutant dispersion will also be

494   reduced. Thus, the weakened entrainment might make the already polluted ABL worse, then a

495   positive feedback between ABL dynamics and pollutant concentration may exist. Quan et al.

496   (2012) proposed that the enhancement of aerosols tends to depress the development of PBL by

497   decreasing solar radiation, while the repressed structure of PBL will in turn weaken the diffusion

498   of pollutants, leading to worsening air quality.

499

500   **4.   Conclusions**

501   Ozone pollution is still an issue in California's urban regions during summer seasons, when

502   wildfires are also prone to happen. The wildfires could not only emit primary pollutants like, CO,

503   NO_x, black carbon, volatile organic compounds, and fine particles, but also provide reactants for

504   the production of secondary pollutants, like O_3. We use data from ten cites in California's

505   Central Valley region in the summers from 2016-2020 and identified wildfire events by HMS

506   system and HYSPLIT model. On average, the wildfire influenced days in CV add up to about 20%

507   of the entire summer time. During wildfire influenced periods, we found that MDA8 O_3

508   increases by 6.5 ppb on average (with about 5 ppb being attributable to the wildfires), and NO_x

509   concentration during daytime increase by 1.1 ppb. The MDA8 O_3 increases with 24-hr $PM_{2.5}$ at

510   low to moderate concentration, peaks at 40-55μg/m^3, and is independent of $PM_{2.5}$ at higher

511   concentrations. From our 5-year data analysis, the percentage of exceeding NAAQS of 70 ppb

512   MDA8 O_3 during wildfire influenced period is about 28% versus only 12% during background

513   periods. Daily maximum temperature and specific humidity show enhancement at most sites,

514   whereas midday windspeed is slightly decreased. The in-situ $P(O_3)$ exhibits enhancement at all

515   sites by 35%, despite $j(NO_2)$ being reduced due to the shading effect of the wildfire plumes. The

516   OPE is also slightly enhanced from which we conclude that the VOCs from wildfire plumes

517   contribute more to the resultant O_3 enhancements than the NO_x, but both of them play a role in

518   increasing O_3 production.

519   The turbulent mixing within the ABL and the ABL height itself have critical impacts on

520   the concentrations of pollutants. We analyze surface heat flux measurements from two

521   AmeriFlux sites located in northern SJV and ABL temperature profile and ABL height from

522   RASS site near Visalia. The surface buoyancy flux decreases by 30% when overhead wildfire

523   plumes are detected. We propose that the decreased surface heat flux is the reason for higher

524   water vapor content and lower windspeed in the ABL. We also found that the midday ABL

525   height decreases by 80 m on average, which matches the SSWD attenuation of 54 W/m^2.

526   Despite the decreased surface heat fluxes, θ_v measurements from RASS show that the ABL

527   becomes 1.5 K warmer on average during wildfire influenced periods. This implies that the

528   ABL dynamics will change due to the presence of wildfire plumes and are the net result of

529   two factors: first, the shading effect of the wildfire plume which decreases the SSWD and

530   surface heat fluxes and consequently reduces the ABL height; and second, the additional

531   aerosols in ABL will absorb more solar radiation and warm the ABL and .

532

533

534

535

536

565 **References**

566 Ainsworth, E. A. (2017). Understanding and improving global crop response to ozone

567   pollution. *The Plant Journal*, *90*(5), 886-897, https://doi.org/10.1111/tpj.13298

568 Akagi, S. K., Yokelson, R. J., Burling, I. R., Meinardi, S., Simpson, I., Blake, D. R., ... &

569   Urbanski, S. (2013). Measurements of reactive trace gases and variable O3 formation rates in

570   some South Carolina biomass burning plumes, https://doi.org/10.5194/acp-13-1141-2013.

571 Alex Valach, Daphne Szutu, Elke Eichelmann, Sara Knox, Joseph Verfaillie, Dennis Baldocchi,

572   Daphne Szutu, Dennis Baldocchi, Elke Eichelmann, Sara Knox (2012-) AmeriFlux US-Tw1

573   Twitchell Wetland West Pond, Dataset. https://doi.org/10.17190/AMF/1246147

574 Alvarado, M. J., Logan, J. A., Mao, J., Apel, E., Riemer, D., Blake, D., ... & Wooldridge, P. J.

575   (2010). Nitrogen oxides and PAN in plumes from boreal fires during ARCTAS-B and their

576   impact on ozone: an integrated analysis of aircraft and satellite observations. *Atmospheric*

577   *Chemistry and Physics*, *10*(20), 9739-9760. https://doi.org/10.5194/acp-10-9739-2010

578 Amann, M. (2008). *Health risks of ozone from long-range transboundary air pollution*. WHO

579   Regional Office Europe.

580 Arya, P. S. (2001). *Introduction to micrometeorology*. Elsevier.

581 Baker, K. R., Woody, M. C., Valin, L., Szykman, J., Yates, E. L., Iraci, L. T., ... & Campuzano-

582   Jost, P. (2018). Photochemical model evaluation of 2013 California wild fire air quality

583   impacts using surface, aircraft, and satellite data. *Science of The Total Environment*, *637*,

584   1137-1149. https://doi.org/10.1016/j.scitotenv.2018.05.048

585 Baylon, P., Jaffe, D. A., Hall, S. R., Ullmann, K., Alvarado, M. J., & Lefer, B. L. (2018). Impact

586   of biomass burning plumes on photolysis rates and ozone formation at the Mount Bachelor

587   Observatory. *Journal of Geophysical Research: Atmospheres*, *123*(4), 2272-2284.

588   https://doi.org/10.1002/2017JD027341

589 Baylon, P., Jaffe, D. A., Wigder, N. L., Gao, H., & Hee, J. (2015). Ozone enhancement in

590   western US wildfire plumes at the Mt. Bachelor Observatory: The role of NOx. *Atmospheric*

591   *Environment*, *109*, 297-304, https://doi.org/10.1016/j.atmosenv.2014.09.013

592 Berkowicz, R., & Prahm, L. P. (1982). Evaluation of the profile method for estimation of surface

593   fluxes of momentum and heat. *Atmospheric Environment (1967)*, *16*(12), 2809-2819,

594   https://doi.org/10.1016/0004-6981(82)90032-4.

595   Bianco, L., Djalalova, I. V., King, C. W., & Wilczak, J. M. (2011). Diurnal evolution and annual

596   variability of boundary-layer height and its correlation to other meteorological variables in

597   California's Central Valley. *Boundary-layer meteorology*, *140*(3), 491-511,

598   DOI: 10.1007/s10546-011-9622-4.

599   Brasseur, G. P., Orlando, J. J., & Tyndall, G. S. (1999). Atmospheric chemistry and global

600   change, (p. 654). New York: Oxford Univ. Press.

601   Brey, S. J., & Fischer, E. V. (2016). Smoke in the city: how often and where does smoke impact

602   summertime ozone in the United States?. *Environmental science & technology*, *50*(3), 1288-

603   1294. https://doi.org/10.1021/acs.est.5b05218

604   Briggs, N. L., Jaffe, D. A., Gao, H., Hee, J. R., Baylon, P. M., Zhang, Q., ... & Cary, R. A.

605   (2016). Particulate matter, ozone, and nitrogen species in aged wildfire plumes observed at

606   the Mount Bachelor Observatory. *Aerosol and Air Quality Research*, *16*(12).

607   DOI: 10.4209/aaqr.2016.03.0120

608   Businger, J. A., Wyngaard, J. C., Izumi, Y., & Bradley, E. F. (1971). Flux-profile relationships in

609   the atmospheric surface layer. *Journal of the atmospheric Sciences*, *28*(2), 181-189,

610   https://doi.org/10.1175/1520-0469(1971)028<0181:FPRITA>2.0.CO;2.

611   Buysse, C. E., Kaulfus, A., Nair, U., & Jaffe, D. A. (2019). Relationships between particulate

612   matter, ozone, and nitrogen oxides during urban smoke events in the western

613   US. *Environmental science & technology*, *53*(21), 12519-12528,

614   https://doi.org/10.1021/acs.est.9b05241

615   Byram, G. M. (1954). Atmospheric conditions related to blowup fires. *Station Paper SE-SP-35.*

616   *Asheville, NC: USDA-Forest Service. Southeastern Forest Experiment Station. 36 p.*, *35*, 1-36.

617   de Gouw, J. A., & Lovejoy, E. R. (1998). Reactive uptake of ozone by liquid organic

618   compounds. *Geophysical Research Letters*, *25*(6), 931-

619   934, https://doi.org/10.1029/98GL00515

620   Dennis Baldocchi, Siyan Ma, Liukang Xu (2000-) AmeriFlux US-Var Vaira Ranch- Ione,

621   Dataset. https://doi.org/10.17190/AMF/1245984

622   Faloona, I. C., Chiao, S., Eiserloh, A. J., Alvarez, R. J., Kirgis, G., Langford, A. O., ... & Yates,

623   E. L. (2020). The California Baseline Ozone Transport Study (CABOTS). *Bulletin of the*

624   *American Meteorological Society*, *101*(4), E427-E445, https://doi.org/10.1175/BAMS-D-18-

625   0302.1.

626 Fischer, E. V., Jaffe, D. A., Reidmiller, D. R., & Jaegle, L. (2010). Meteorological controls on

627   observed peroxyacetyl nitrate at Mount Bachelor during the spring of 2008. *Journal of*

628   *Geophysical Research: Atmospheres*, *115*(D3). https://doi.org/10.1029/2009JD012776

629 Griffin, R. J., Beckman, P. J., Talbot, R. W., Sive, B. C., & Varner, R. K. (2007). Deviations

630   from ozone photostationary state during the International Consortium for Atmospheric

631   Research on Transport and Transformation 2004 campaign: Use of measurements and

632   photochemical modeling to assess potential causes. *Journal of Geophysical Research:*

633   *Atmospheres*, *112*(D10). https://doi.org/10.1029/2006JD007604

634 Högström, U. L. F. (1996). Review of some basic characteristics of the atmospheric surface

635   layer. *Boundary-Layer Meteorology*, *78*(3-4), 215-246, https://doi.org/10.1007/BF00120937.

636 Jaffe, D. A., & Wigder, N. L. (2012). Ozone production from wildfires: A critical

637   review. *Atmospheric Environment*, *51*, 1-10. https://doi.org/10.1016/j.atmosenv.2011.11.063

638 Kaulfus, A. S., Nair, U., Jaffe, D., Christopher, S. A., & Goodrick, S. (2017). Biomass burning

639   smoke climatology of the United States: Implications for particulate matter air

640   quality. *Environmental Science & Technology*, *51*(20), 11731-11741,

641   https://doi.org/10.1021/acs.est.7b03292.

642 Laing, J. R., Jaffe, D. A., Slavens, A. P., Li, W., & Wang, W. (2017). Can d; PM2. 5/d; CO and d;

643   NOy/d; CO Enhancement Ratios Be Used to Characterize the Influence of Wildfire Smoke in

644   Urban Areas?. *Aerosol and Air Quality Research*, *17*(10), 2413-2423.

645   https://doi.org/10.4209/aaqr.2017.02.0069

646 Langford, A. O., Alvarez, R. J., Brioude, J., Caputi, D., Conley, S. A., Evan, S., et al. (2020).

647   Ozone production in the Soberanes smoke haze: Implications for air quality in the San

648   Joaquin Valley during the California Baseline Ozone Transport Study. *Journal of*

649   *Geophysical Research: Atmospheres*, 125, e2019JD031777.

650   https://doi.org/10.1029/2019JD031777

651 Leighton, P. A. Photochemistry of Air Pollution. *Academic Press: New York*, 1961, Vol. 9.

652 Leukauf, D., Gohm, A., & Rotach, M. W. (2016). Quantifying horizontal and vertical tracer mass

653   fluxes in an idealized valley during daytime. *Atmospheric Chemistry and Physics*, *16*(20),

654   13049. https://doi.org/10.5194/acp-16-13049-2016

655 Lin, M., Horowitz, L. W., Payton, R., Fiore, A. M., & Tonnesen, G. (2017). US surface ozone

656   trends and extremes from 1980 to 2014: quantifying the roles of rising Asian emissions,

657   domestic controls, wildfires, and climate. *Atmospheric Chemistry & Physics*, *17*(4),

658   https://doi.org/10.5194/acp-17-2943-2017, 2017.

659 Lin, X., Trainer, M., & Liu, S. C. (1988). On the nonlinearity of the tropospheric ozone

660   production. *Journal of Geophysical Research: Atmospheres*, *93*(D12), 15879-

661   15888. https://doi.org/10.1029/JD093iD12p15879

662 Lippmann, H. H., Jesser, B., & Schurath, U. (1980). The rate constant of NO+ O3→ NO2+ O2

663   in the temperature range of 283–443 K. *International Journal of Chemical Kinetics*, *12*(8),

664   547-554, https://doi.org/10.1002/kin.550120805

665 Liu, C., Fedorovich, E., Huang, J., Hu, X. M., Wang, Y., & Lee, X. (2019). Impact of aerosol

666   shortwave radiative heating on entrainment in the atmospheric convective boundary layer: A

667   large-eddy simulation study. *Journal of the Atmospheric Sciences*, *76*(3), 785-799.

668   https://doi.org/10.1175/JAS-D-18-0107.1

669 Liu, S. C., Trainer, M., Fehsenfeld, F. C., Parrish, D. D., Williams, E. J., Fahey, D. W., ... &

670   Murphy, P. C. (1987). Ozone production in the rural troposphere and the implications for

671   regional and global ozone distributions. *Journal of Geophysical Research:*

672   *Atmospheres*, *92*(D4), 4191-4207. https://doi.org/10.1029/JD092iD04p04191

673 Mannschreck, K., Klemp, D., Kley, D., Friedrich, R., Kühlwein, J., Wickert, B., ... & Slemr, F.

674   (2002). Evaluation of an emission inventory by comparisons of modelled and measured

675   emission ratios of individual HCs, CO and NOx. *Atmospheric Environment*, *36*, 81-94.

676   https://doi.org/10.1016/S1352-2310(02)00211-X

677 Martin, M. V., Honrath, R. E., Owen, R. C., Pfister, G., Fialho, P., & Barata, F. (2006).

678   Significant enhancements of nitrogen oxides, black carbon, and ozone in the North Atlantic

679   lower free troposphere resulting from North American boreal wildfires. *Journal of*

680   *Geophysical Research: Atmospheres*, *111*(D23), https://doi.org/10.1029/2006JD007530

681 McClure, C. D., & Jaffe, D. A. (2018). Investigation of high ozone events due to wildfire smoke

682   in an urban area. *Atmospheric Environment*, *194*, 146-157,

683   https://doi.org/10.1016/j.atmosenv.2018.09.021

684 Monin, A. S., & Obukhov, A. M. (1953). Dimensionless characteristics of turbulence in the

685   atmospheric surface layer. In *Dokl. Akad. Nauk SSSR* (Vol. 93, No. 2, pp. 223-226).

686   Olszyna, K. J., Bailey, E. M., Simonaitis, R., & Meagher, J. F. (1994). O3 and NO y

687   relationships at a rural site. *Journal of Geophysical Research: Atmospheres*, *99*(D7), 14557-

688   14563. https://doi.org/10.1029/94JD00739

689   Pahlow, M., Kleissl, J., & Parlange, M. B. (2005). Atmospheric boundary-layer structure

690   observed during a haze event due to forest-fire smoke. *Boundary-layer meteorology*, *114*(1),

691   53-70, DOI: 10.1007/s10546-004-6350-z.

692   Pal, S., & Haeffelin, M. (2015). Forcing mechanisms governing diurnal, seasonal, and

693   interannual variability in the boundary layer depths: Five years of continuous lidar

694   observations over a suburban site near Paris. *Journal of Geophysical Research:*

695   *Atmospheres*, *120*(23), 11-936. https://doi.org/10.1002/2015JD023268

696   Parrish, D. D., Trainer, M., Holloway, J. S., Yee, J. E., Warshawsky, M. S., Fehsenfeld, F. C., ...

697   & Moody, J. L. (1998). Relationships between ozone and carbon monoxide at surface sites in

698   the North Atlantic region. *Journal of Geophysical Research: Atmospheres*, *103*(D11), 13357-

699   13376, https://doi.org/10.1029/98JD00376

700   Pusede, S. E., Gentner, D. R., Wooldridge, P. J., Browne, E. C., Rollins, A. W., Min, K. E., ... &

701   Henry, S. B. (2014). On the temperature dependence of organic reactivity, nitrogen oxides,

702   ozone production, and the impact of emission controls in San Joaquin Valley,

703   California. *Atmospheric Chemistry and Physics*, *14*(7), 3373-3395.

704   https://doi.org/10.5194/acp-14-3373-2014, 2014.

705   Quan, Jiannong, et al. "Evolution of planetary boundary layer under different weather conditions,

706   and its impact on aerosol concentrations." *Particuology* 11.1 (2013): 34-40. DOI:

707   10.1016/j.partic.2012.04.005

708   Reid, J. S., Koppmann, R., Eck, T. F., & Eleuterio, D. P. (2005). A review of biomass burning

709   emissions part II: intensive physical properties of biomass burning particles. *Atmospheric*

710   *Chemistry and Physics*, *5*(3), 799-825, https://doi.org/10.5194/acp-5-799-2005.

711   Rombout, P. J., Lioy, P. J., & Goldstein, B. D. (1986). Rationale for an eight-hour ozone

712   standard. *Journal of the Air Pollution Control Association*, *36*(8), 913-917,

713   https://doi.org/10.1080/00022470.1986.10466130

714   Rothermel, R. (1991). Predicting the Behaviour and Size of Crown Fires in the Northern Rocky

715   Mountains-USDA-FS. *Res. Pap. INT-359*.

716 Sillman, S., & Samson, P. J. (1995). Impact of temperature on oxidant photochemistry in urban,

717   polluted rural and remote environments. *Journal of Geophysical Research:*

718   *Atmospheres*, *100*(D6), 11497-11508. https://doi.org/10.1029/94JD02146

719 Singh, H. B., Cai, C., Kaduwela, A., Weinheimer, A., & Wisthaler, A. (2012). Interactions of fire

720   emissions and urban pollution over California: Ozone formation and air quality

721   simulations. *Atmospheric Environment*, *56*, 45-51,

722   https://doi.org/10.1016/j.atmosenv.2012.03.046

723 Stavros, E. N., Abatzoglou, J. T., McKenzie, D., & Larkin, N. K. (2014). Regional projections of

724   the likelihood of very large wildland fires under a changing climate in the contiguous Western

725   United States. *Climatic Change*, *126*(3-4), 455-468, https://doi.org/10.1007/s10584-014-

726   1229-6.

727 Stull, R. B. (1988). *An introduction to boundary layer meteorology* (Vol. 13). Springer Science

728   & Business Media.

729 Tan, Z., Lu, K., Dong, H., Hu, M., Li, X., Liu, Y., ... & Wu, Y. (2018). Explicit diagnosis of the

730   local ozone production rate and the ozone-NOx-VOC sensitivities. *Science bulletin*, *63*(16),

731   1067-1076. https://doi.org/10.1016/j.scib.2018.07.001

732 Trainer, M., Parrish, D. D., Buhr, M. P., Norton, R. B., Fehsenfeld, F. C., Anlauf, K. G., ... &

733   Tanner, R. L. (1993). Correlation of ozone with NOy in photochemically aged air. *Journal of*

734   *Geophysical Research: Atmospheres*, *98*(D2), 2917-2925. https://doi.org/10.1029/92JD01910

735 Trebs, I., Bohn, B., Ammann, C., Rummel, U., Blumthaler, M., Königstedt, R., ... & Andreae, M.

736   O. (2009). Relationship between the NO 2 photolysis frequency and the solar global

737   irradiance. *Atmospheric Measurement Techniques*, *2*(2), 725-739.

738   https://doi.org/10.5194/amt-2-725-2009, 2009.

739 Trousdell, Justin F., Stephen A. Conley, Andy Post, and Ian C. Faloona. "Observing entrainment

740   mixing, photochemical ozone production, and regional methane emissions by aircraft using a

741   simple mixed-layer framework." *Atmospheric Chemistry and Physics* 16, no. 24 (2016):

742   15433-15450. https://doi.org/10.5194/acp-16-15433-2016

743 Volz-Thomas, A., Pätz, H. W., Houben, N., Konrad, S., Mihelcic, D., Klüpfel, T., & Perner, D.

744   (2003). Inorganic trace gases and peroxy radicals during BERLIOZ at Pabstthum: An

745   investigation of the photostationary state of NOx and O3. *Journal of Geophysical Research:*

746   *Atmospheres*, *108*(D4), PHO-4. https://doi.org/10.1029/2001JD001255

747 Wendisch, M., Mertes, S., Ruggaber, A., & Nakajima, T. (1996). Vertical profiles of aerosol and

748   radiation and the influence of a temperature inversion: Measurements and radiative transfer

749   calculations. *Journal of Applied Meteorology*, *35*(10), 1703-1715,

750   https://doi.org/10.1175/15200450(1996)035<1703:VPOAAR>2.0.CO;2

751 Yokelson, R. J., Crounse, J. D., DeCarlo, P. F., Karl, T., Urbanski, S., Atlas, E., ... &

752   Weinheimer, A. (2009). Emissions from biomass burning in the Yucatan.

753   http://dx.doi.org/10.5194/acp-9-5785-2009

754 Zhang, L., Jacob, D. J., Yue, X., Downey, N. V., Wood, D. A., & Blewitt, D. (2014). Sources

755   contributing to background surface ozone in the US Intermountain West. *Atmospheric*

756   *Chemistry and Physics*, https://doi.org/10.5194/acp-14-5295-2014

757
758
759
760
761
762
763
764
765
766
767
768
769
770
771
772
773
774
775
776
777
778
779
780
781
782
783
784
785
786
787
788
789
790
791
792
793
794

Tables

Table 1. *Measurement sites location and detail information in this study.*

Site Name	Site Location (°N, °E)	Agency	Measurements
Chico-East	39.76, -121.84	CARB	O_3, $PM_{2.5}$, CO, NO, NO_2, T, RH
MADIS-KCIC	39.80, -121.85	MADIS	U, RH (2016)
Yuba City	39.14, -121.62	CARB	O_3, $PM_{2.5}$, NO, NO_2, T, RH
MADIS-KMYV	39.10, -121.57	MADIS	U, P, RH (2016-2017)
Sutter Buttes	39.21, -121.82	CARB	CO (2017-2019)
Arden Arcade - Del Paso Manor	38.61, -121.37	Sacramento Metro. AQMD	O_3, $PM_{2.5}$, CO (2016-2019), NO, NO_2, T, RH, U, P
Stockton - Hazelton Street	37.95, -121.27	CARB	O_3, $PM_{2.5}$, CO, NO, NO_2, T, RH
MADIS-KSCK	37.90, -121.25	MADIS	U, P, RH (2016)
Modesto - 14th Street	37.64, -120.99	CARB	O_3, $PM_{2.5}$, CO, T, RH
MADIS-KMOD	37.63, -120.95	MADIS	U, P, RH (2016)
Merced - S. Coffee Ave	37.28, -120.43	CARB	O_3, $PM_{2.5}$, NO, NO_2, T, RH, U
Madera-City	36.95, -120.03	San Joaquin Valley Unified APCD	P, $PM_{2.5}$
Madera - Pump Yard	36.87, -120.01	San Joaquin Valley Unified APCD	O_3, CO, NO, NO_2, T, RH, U
Fresno - Garland	36.79, -119.77	CARB	O_3, $PM_{2.5}$, CO, NO, NO_2, T, RH
MADIS-KFAT	36.77, -119.72	MADIS	U, P, RH (2016)
Visalia - N. Church Street	36.33, -119.29	CARB	O_3, $PM_{2.5}$, NO, NO_2, T, RH
MADIS-KVIS	36.32, -119.40	MADIS	U, P, RH (2016)

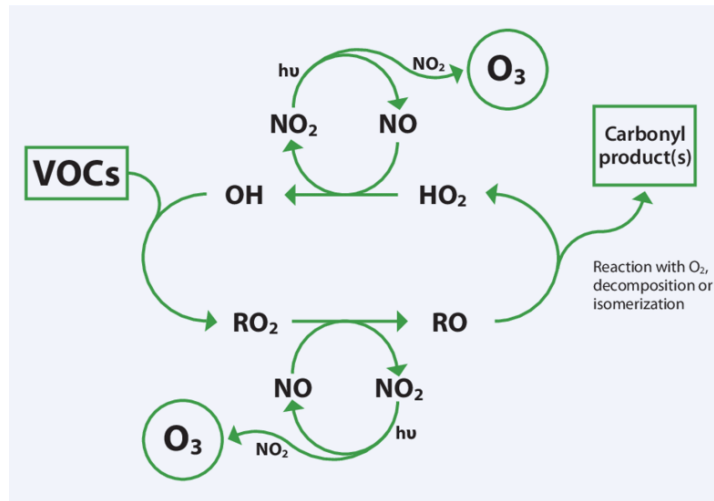|			
Bakersfield - California Ave	35.36, -119.06	CARB	$PM_{2.5}$
Bakersfield-Muni	35.33, -119.00	San Joaquin Valley Unified APCD	O_3, CO, NO, NO_2, T, RH, U, P

797

798

799

800

801

802

803

804

805

806

807

808

809

810 **Figures**

811 *Figure 1.* Schematic representation of the photochemical formation of ozone in the presence of NO_x and VOCs
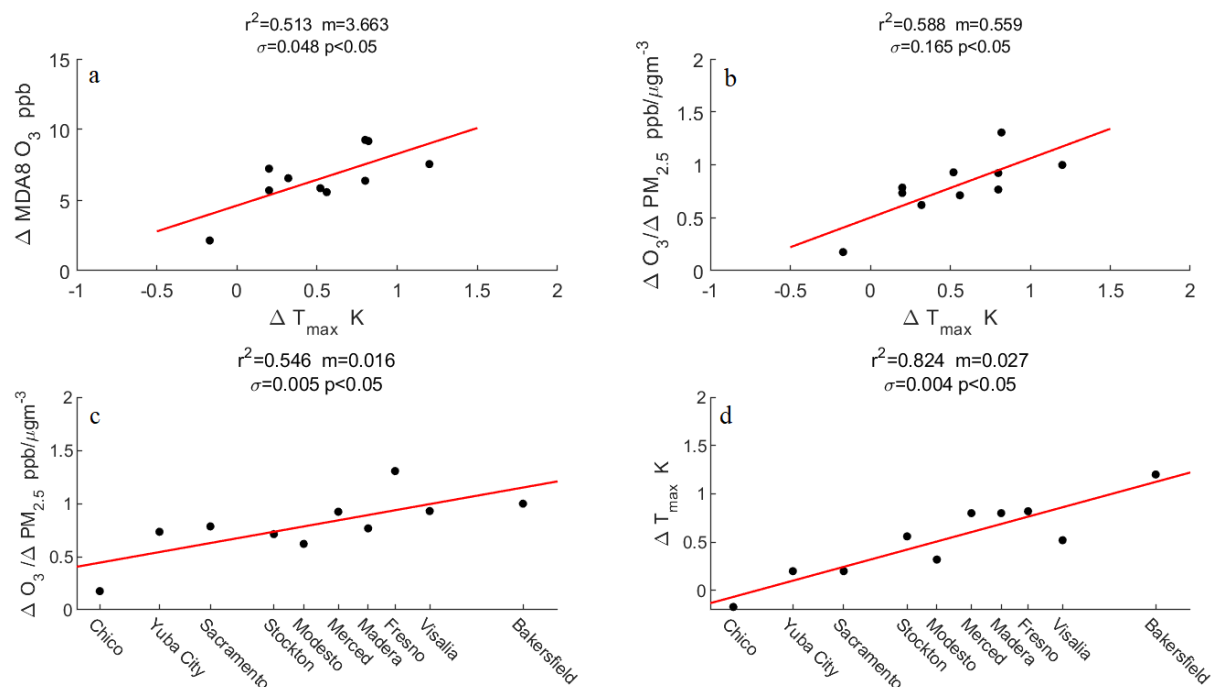
812 *(Amann, 2018)*

813

814

815

816

817

818

819

820

821

822

823

824

825

826

827

828

829
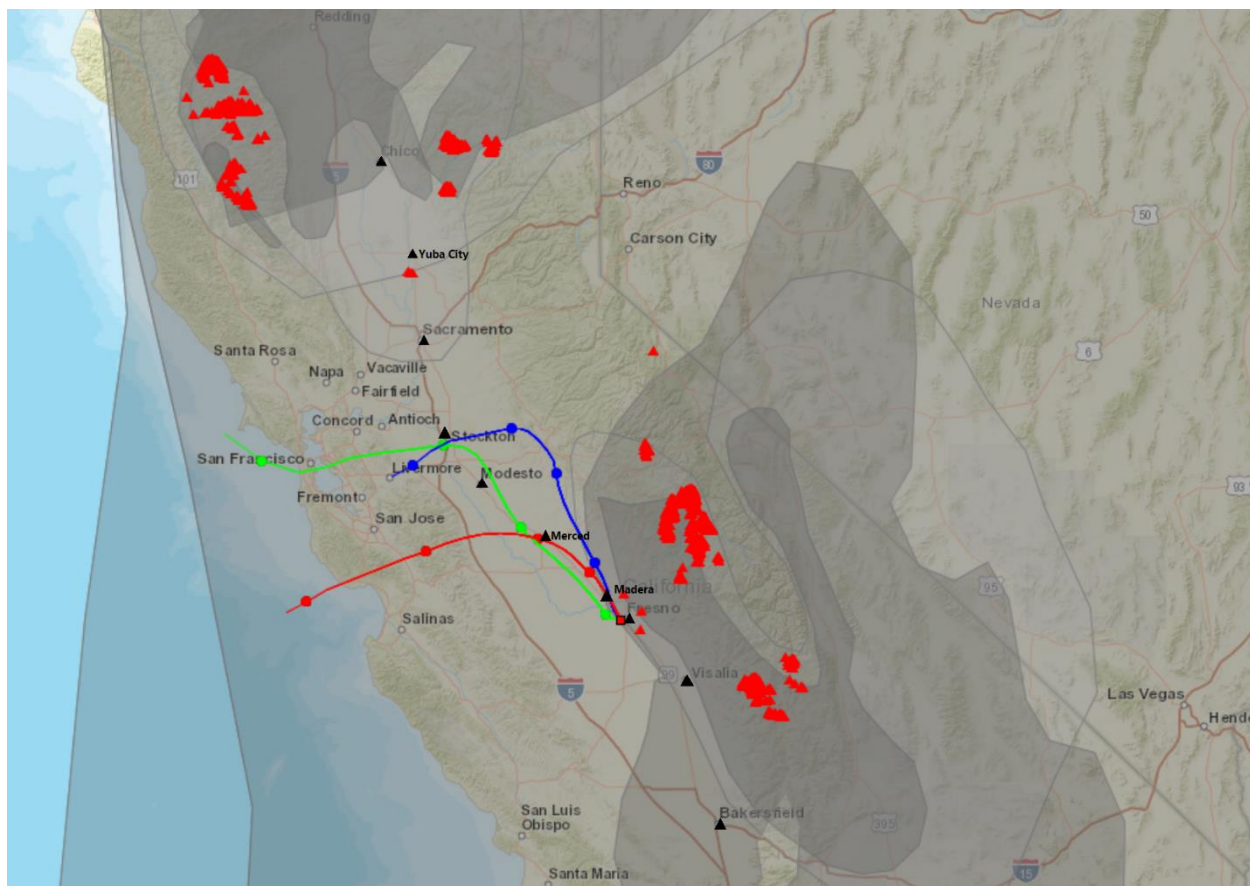
Figure 2. *A snapshot of HMS product on 12:00 PST 23 September 2020, where red triangles are fire locations,*

black triangles are the sites we chose, the shading areas represent wildfire coverage, and the thickness of the plume

is indicated by the color of the shade. The colored lines represent 24 hours HYSPLIT back-trajectory performed at

Fresno at the altitude of 100m (green), 600m (blue), and 1500m (red), respectively. The dots on the line represent a

6-hour time interval.

835

836

837

838

839

840

841

842
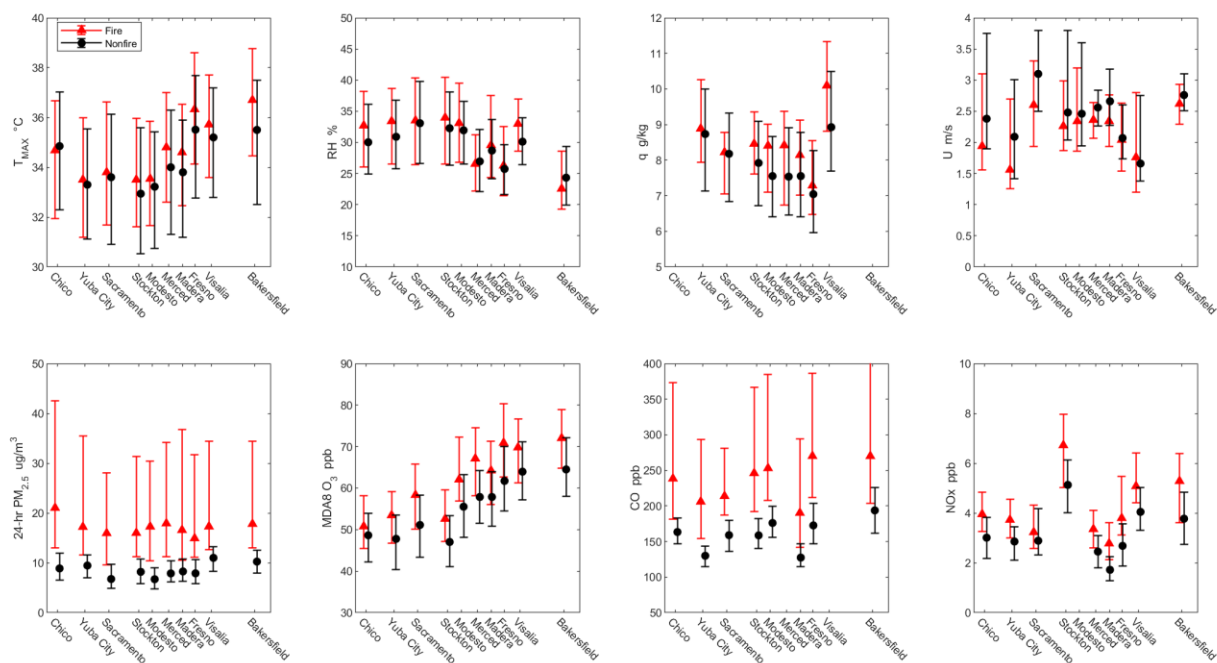
843   ***Figure 3.*** *Median value for fire (red triangle) and non-fire (black circle) periods at each station, error bars*

844   *represent 25th and 75th percentile. RH, q, P(O$_3$), CO and NOx values are 5-hour averaged value between 10:00 to*

845   *15:00 PST. The interval of X-axis label is proportional to the latitude of each site.*

846

847

848

849

850

851

852

853

854

855

856 **Figure 4.** *Enhancement ratio of MDA8 O_3 to T_{max} (a), 24-hr $PM_{2.5}$ (c) and ΔT_{max} (d) at each site. ER ratio of MDA8*

857 *O_3/24-hr $PM_{2.5}$ respect to ΔT_{max} (b). Enhancements are the differences in median values between wildfire and*

858 *background periods. The σ is the standard error for the linear regression, p is the P-value that represent the*

859 *rejection of null hypothesis. The interval of X-axis label is proportional to the latitude of each site.*

860

861

862

863

864

865

866

867

868
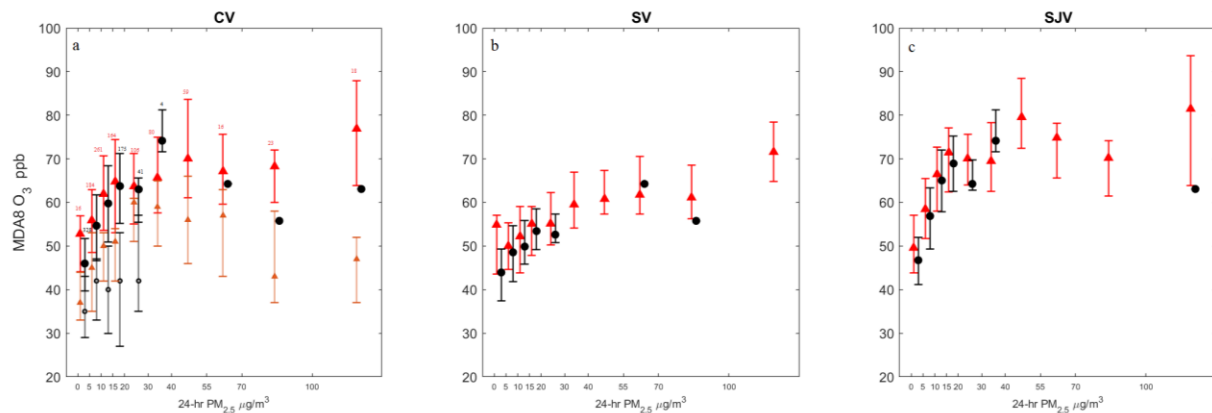
Figure 5. *Plots for binned 24-hr PM$_{2.5}$ versus MDA8 O$_3$ for all ten sites (a); Chico, Yuba City, and Sacramento are in (b); and sites in SJV are in (c), black dots and red triangles denote median value for background and wildfire period, respectively. Error bars denote 25th and 75th percentile. The number of datapoints are display on the top of each bins. The orange (fire) and grey (non-fire) error bars are result from Buysee et al. (2019) for comparison.*

873

874

875

876

877

878

879

880

881

882

883
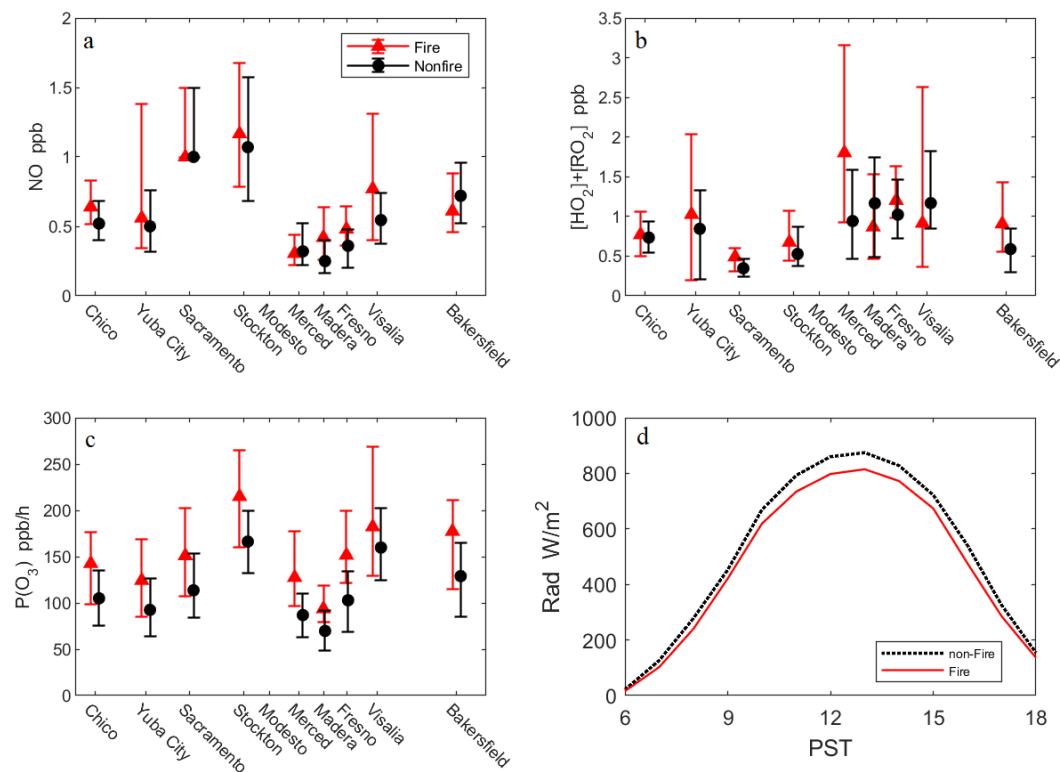
884 **Figure 6.** *Plots for NO (a), [RO$_2$]+[HO$_2$] (b), PO$_3$ (c) at each site, and averaged SSWD (d). The red circle*

885 *and black dot represent median value for 5-hour average between 10:00 and 15:00 PST during wildfire and*
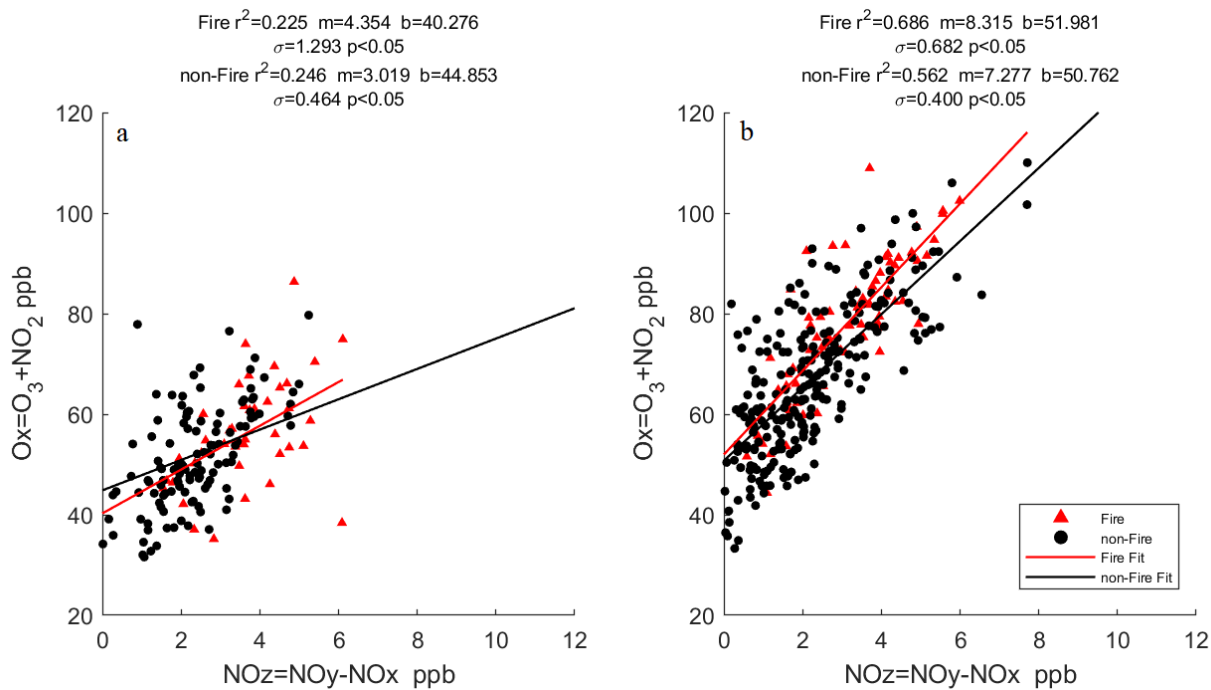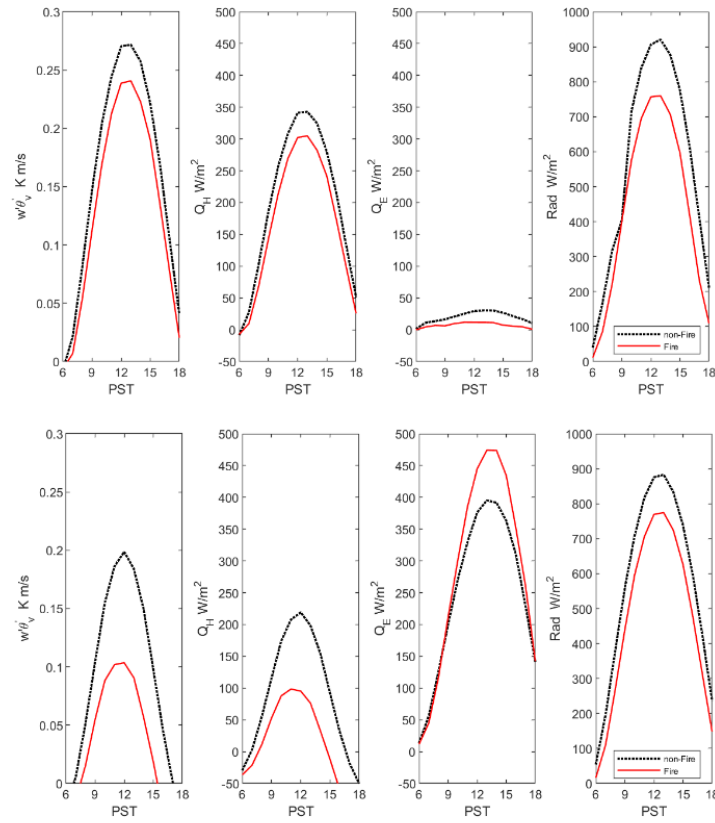
886 *background days.*

887

888

889

890

891

892

893

894

895 **Figure 7.** *Scatter plot of O_x versus NO_z at Sacramento (a) and Fresno (b). The slope of the linear regression (m)*

896 *represents the OPE. The σ is the standard error for the linear regression, p is the P-value that represent the*

897 *rejection of null hypothesis.*

898

899

900

901

902

903

904

905

906

907 ***Figure 8.*** *Measurements of buoyancy flux (*$w'\theta'_v$*), sensible heat flux (*Q_H*), latent heat flux (*Q_E*), and*

908 *incoming solar radiation (SSWD) at Vaira Ranch (top) and Twitchell Wetland (bottom). Black dash lines are*

909 *the diurnal profile for non-fire days and red lines are profiles during wildfire periods (Jun-Sep) from 2016*
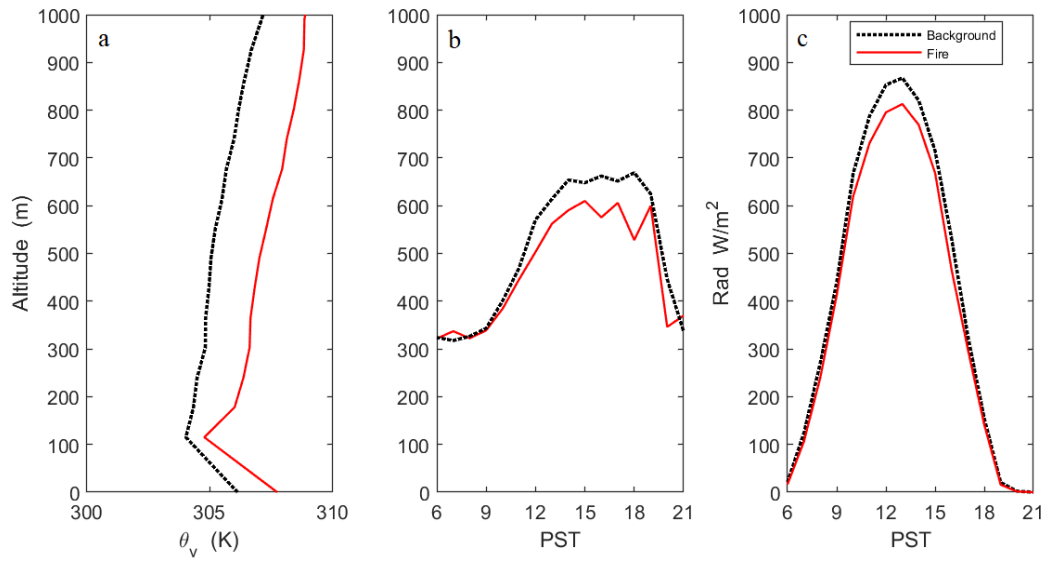
910 *to 2019.*

911

912

913

914

915

916   ***Figure 9.*** *Averaged diurnal profile for daytime ABL height (b), virtual potential temperature (θ$_v$) profile*

917   *between 13:00 and 15:00 PST (a), and diurnal SSWD profile (c) at Visalia during wildfire days (red) and*

918   *background periods (black) from 2016 to 2020.*

919

920

921

922

923

924

925

926

927

928